

1 **SARS-CoV-2 mRNA vaccine is re-adenylated *in vivo*, enhancing antigen production and immune**
2 **response**

3
4 **Authors:** Paweł S Krawczyk¹, Olga Gewartowska^{1,*}, Michał Mazur^{1,*}, Wiktoria Orzeł^{1,2,*}, Katarzyna
5 Matylla-Kulińska^{1,2}, Sebastian Jeleń^{1,2}, Paweł Turowski³, Tomasz Śpiewła⁴, Bartosz Tarkowski¹,
6 Agnieszka Tudek⁵, Aleksandra Brouze^{1,2}, Aleksandra Wesołowska⁶, Dominika Nowis⁷, Jakub Gołąb⁸,
7 Joanna Kowalska⁴, Jacek Jemielity⁹, Andrzej Dziembowski^{1,2,#}, and Seweryn Mroczek^{2,1,#}

8 **Affiliations**

9 ¹ International Institute of Molecular and Cell Biology, 4 Ks. Trojdena, 02-106 Warsaw, Poland.

10 ² Faculty of Biology, University of Warsaw, 5a Pawinskiego, 02-106, Warsaw, Poland

11 ³ ExploRNA Therapeutics, 101 Żwirki i Wigury, 02-089, Warsaw, Poland

12 ⁴ Faculty of Physics, University of Warsaw, Pasteura 5, 02-093, Warsaw, Poland

13 ⁵ Institute of Biochemistry and Biophysics, 5A Pawińskiego, 02-106 Warsaw, Poland

14 ⁶ Department of Medical Biology, Medical University of Warsaw, Litewska 14/16, 00-575, Warsaw, Poland

15 ⁷ Laboratory of Experimental Medicine, Medical University of Warsaw, 5 Nielubowicza Str., 02-097,
16 Warsaw, Poland.

17 ⁸ Department of Immunology, Medical University of Warsaw, 5 Nielubowicza Str., 02-097, Warsaw,
18 Poland.

19 ⁹ Centre of New Technologies, University of Warsaw, Banacha 2c, 02-097, Warsaw, Poland

20 * contributed equally

21 # corresponding authors

22

23 **Abstract**

24 Though mRNA vaccines against COVID-19 have revolutionized vaccinology and have been administered
25 in billions of doses, we know incredibly little about how mRNA vaccines are metabolized *in vivo*. Here we
26 implemented enhanced nanopore Direct RNA sequencing (eDRS), to enable the analysis of single
27 Moderna's mRNA-1273 molecules, giving *in vivo* information about the sequence and poly(A) tails.

28 We show that mRNA-1273, with all uridines replaced by N1-methylpseudouridine (m Ψ), is terminated by
29 a long poly(A) tail (~100 nucleotides) followed by an m Ψ Cm Ψ AG sequence. In model cell lines, mRNA-
30 1273 is swiftly degraded in a process initiated by the removal of m Ψ Cm Ψ AG, followed by CCR4-NOT-
31 mediated deadenylation. In contrast, intramuscularly inoculated mRNA-1273 undergoes more complex
32 modifications. Notably, mRNA-1273 molecules are re-adenylated after m Ψ Cm Ψ AG removal. Detailed
33 analysis of immune cells involved in antigen production revealed that in macrophages, after m Ψ Cm Ψ AG
34 removal, vaccine mRNA is very efficiently re-adenylated, and poly(A) tails can reach up to 200A. In
35 contrast, in dendritic cells, vaccine mRNA undergoes slow deadenylation-dependent decay. We further
36 demonstrate that enhancement of mRNA stability in macrophages is mediated by TENT5 poly(A)
37 polymerases, whose expression is induced by the vaccine itself. Lack of TENT5-mediated re-adenylation
38 results in lower antigen production and severely compromises specific immunoglobulin production
39 following vaccination.

40 Together, our findings provide an unexpected principle for the high efficacy of mRNA vaccines and open
41 new possibilities for their improvement. They also emphasize that, in addition to targeting a protein of
42 interest, the design of mRNA therapeutics should be customized to its cellular destination.

43

44 **Keywords :** mRNA vaccine, mRNA-1273, Direct RNA sequencing, poly(A), TENT5A, TENT5C, immune
45 response, CCR4-NOT, polyadenylation, deadenylation

46

47 **Main**

48 The worldwide pandemic thrust vaccine development, and specifically development of mRNA-based
49 vaccines. Thankfully for humankind, mRNA vaccines were deployed at an almost unimaginable speed and
50 at worldwide scale.

51 Though pressed into immediate action, the mRNA vaccine field is still at very early stages. As this method
52 of vaccine design was entirely new, it is essentially unknown how cellular and organismal systems respond
53 to administration of an mRNA vaccine. Successful targeting of an mRNA vaccine, such as that against the
54 SARS-CoV-2 spike protein, could be vastly improved by understanding the systems responsible for
55 disseminating the vaccine in the body; uptake of the exogenous mRNA in different cell types; how or if
56 mRNA inside the cell is maintained or metabolized; and how the protein product of the mRNA is used to
57 build an immune reaction.

58 Clarification and harnessing of even some of these factors could make a significant difference in the efficacy
59 and utility of mRNA vaccines. These factors could be of critical importance for reducing the ongoing
60 burden of COVID-19, and also be broadly applied to improve the action and efficacy of many viral agents.

61 The most potent vaccines for combating COVID-19 (BNT162b2 and mRNA-1273) to date are based on *in*
62 *vitro*-transcribed (IVT) mRNA^{1,2}. mRNA vaccines are administered encapsulated in lipid nanoparticles
63 (LNPs) and enter cells mainly by endocytic pathways^{3,4}. A fraction of these payloads is released from
64 endosomes to the cytosol, where protein production occurs. Intramuscularly administered mRNA vaccines
65 transfect neighboring resident immune cells, such as antigen-presenting dendritic cells (DCs) and
66 macrophages. These cells become activated and migrate to neighboring lymph nodes⁵⁻⁸. LNPs, as well as
67 secreted antigens produced in muscles, are also transported to local lymph nodes, where they are taken up
68 by macrophages and resident DCs^{8,9}. Although not directly demonstrated, it is likely that vaccine antigens
69 transported with lymph and/or locally produced in the lymph nodes are stored on the surface of follicular
70 DCs and induce a humoral immune response. DCs, which are central for adaptive immunity, endocytose
71 antigens produced by other cells and translate vaccine mRNAs⁹. Peptide antigens are presented in

72 association with class I and class II MHC molecules to T cells to induce effector CD8⁺ and CD4⁺ T cells^{4,8}.
73 The latter include helper (Th1) and follicular helper T (Tfh1) cells that are involved in the regulation of
74 antiviral immunity in the periphery and development of humoral immune response in the follicles,
75 respectively⁸. Many studies on mRNA vaccines have focused on DCs^{10,11}. However, though
76 macrophages/monocytes are the main cell population that take up mRNA vaccines^{5,8}, their role in mRNA
77 vaccine efficacy is not well defined.

78 Therapeutic mRNA resembles normal mRNA, having both a cap structure and poly(A) tail³, but it is
79 generated through *in vitro* transcription, usually by T7 polymerase on a DNA template. A breakthrough in
80 the development of RNA therapeutics came with the discovery that replacement of uridine with N1-methyl-
81 pseudouridine (m Ψ) decreases the innate immune response and enhances mRNA stability¹²⁻¹⁵. Although
82 most currently synthesized mRNA therapeutics contain this modification, exceptions show it is not
83 essential^{16,17}. The two worldwide-approved mRNA vaccines, Bnt162b2^{2,18} and mRNA-1273^{1,19}, encoding
84 coronaviral spike protein (S protein), are produced using IVT and have all uridines replaced with m Ψ , as
85 well as a similar 5' cap that is incorporated co-transcriptionally for Bnt162b2 and post-transcriptionally for
86 mRNA-1273. However, they differ in their UTR sequences and 3' tails²⁰. Bnt162b2 vaccine has a composite
87 poly(A) tail, with 30As followed by 10 other nucleotides, and then 70 additional As¹⁸, whereas mRNA-
88 1273 has a poly(A) tail of undisclosed length. Both vaccines are formulated into nanoparticles with a similar
89 lipid composition. The immune response was characterized for primary, secondary, and third dose
90 vaccinations^{19,21}, showing potent protection against the original variants, but also against variants of concern
91 (VOC).

92 Knowledge about *in vivo* and *in-cell* metabolism of mRNA vaccines is extremely limited and is largely
93 based on extrapolation from experiments in established cell lines with generic mRNAs. The paradigm
94 extrapolated from data obtained on endogenous transcripts (or reporters) asserts that the stability of
95 therapeutic mRNAs is determined by the rate of poly(A) tail removal (deadenylation). Notably, almost
96 nothing is known regarding the metabolism of vaccines' poly(A) tails. Herein, we implement nanopore

97 direct RNA sequencing for a detailed dissection of mRNA-1273, revealing the complexity of its
98 metabolism. Importantly, we show that mRNA-1273 is stabilized in macrophages by TENT5-mediated re-
99 adenylation. We further demonstrate that TENT5A enhances the expression of the mRNA-1273 antigen *in*
100 *vivo*, which is essential for an efficient immune response. Notably, in the past, the action of the endogenous
101 polyadenylation machinery on mRNA therapeutics has not been reported or even considered.

102

103 **Direct RNA sequencing of mRNA vaccines**

104 Studies of therapeutic mRNA metabolism face methodological challenges and, consequently, knowledge
105 about the *in vivo* metabolism of mRNA vaccines is sparse. Approaches based on sequencing are usually
106 indirect and rely on analysis of PCR-amplified cDNA. For poly(A) tails, such studies are error-prone, due
107 to polymerase slipping on homopolymers. Similar problems concern the quality control of mRNA
108 therapeutics, especially their poly(A) tails. Direct RNA sequencing (DRS, Oxford Nanopore
109 Technologies¹⁸) has the potential to overcome technical barriers, as it is based on detecting electric current
110 during the passage of single ssRNA molecules through a protein pore. Thus, DRS can provide reliable
111 information on RNA composition with single-molecule resolution. However, the replacement of uridine
112 with m Ψ in mRNA therapeutics poses additional challenges, as this substitution perturbs current signal
113 recorded during DRS and can result in imprecise translation into sequence (basecalling)²³.

114 Analysis of intact mRNA-1273 using a standard DRS pipeline (**Fig. 1a**) showed that a significant proportion
115 of aligned reads covered the full-length vaccine (**Fig. 1b**, blue), showing promise for comprehensive
116 analysis of mRNA therapeutics via DRS. However, these experiments confirmed that m Ψ indeed affects
117 the basecalling process [Extended Data (ED) Fig 1a)]. Only 35.74% of reads aligned to the reference
118 vaccine sequence, and those aligned reads had only 74.1% identity to the reference. Thus, the current data
119 analysis pipeline is presently unsuitable for m Ψ modified mRNAs.

120 To improve our ability to identify desired reads, we developed a subsequence Dynamic Time Warping
121 (sDTW) approach (ED Fig. 1b), to identify ionic current signatures specific to the 3' end of mRNA-1273.

122 This method, in principle, is similar to targeted nanopore sequencing²⁴ and independent of basecalling and
123 mapping. Compared to mapping alone, a combination of sDTW with mapping allowed the identification of
124 twice as many sequences (ED Fig. 1c), validating the feasibility and promise of this approach. It was
125 especially valuable for identifying shorter, lower-quality 3'-terminal reads (ED Fig. 1d), which would have
126 been missed otherwise.

127 Next, we focused on improving accuracy in the determination of vaccine poly(A) tails, which are essential
128 for mRNA stability and translation. Initially, we employed the nanopolish-polya algorithm to identify and
129 measure poly(A) tails²⁵, with good accuracy (ED Fig. 1e). This study revealed that mRNA-1273 has a
130 poly(A) tract of ~100 adenosines (**Fig. 1c**, ED Fig. 1f). However, visual inspection of the raw current
131 revealed unexpected perturbation between the poly(A) tail and the adaptor used for library preparation (**Fig.**
132 **1d**, bottom panel, green). Such a signal suggests the presence of terminal non-adenosine residue(s) in the
133 mRNA-1273 vaccine. To verify whether this signature is specific to the 3' end of mRNA-1273, and not
134 introduced during library preparation, we repeated the experiments with a vaccine RNA whose 3' end was
135 enzymatically extended with inosine nucleotides (I-tailing), followed by direct RNA sequencing with a
136 custom protocol enabling the incorporation of such RNAs into the library. This analysis reproduced the
137 same current perturbation (ED Fig. 1g).

138 Finally, Rapid Amplification of cDNA 3' End (3'-RACE) Illumina sequencing revealed the presence of
139 TCTAG (mΨCmΨAG in vaccine mRNA) (**Fig. 1e**), which likely represents the residue of restriction
140 enzyme cleavage of the DNA template. For quantitative studies of mRNA-1273, we generated an enhanced
141 DRS pipeline (eDRS) incorporating sDTW and a modified algorithm for the detection of poly(A) tails with
142 mΨCmΨAG. Analysis of intact vaccine RNA showed that the major fraction of vaccine RNA molecules
143 had an intact 3' end. We observed that roughly 20% of the analyzed reads lacked the mΨCmΨAG sequence
144 (**Fig. 1c**, red, bottom panel) and were characterized by a broader distribution of poly(A) lengths (**Fig. 1c**,
145 red, upper panel). We propose that the eDRS pipeline is well suited to the analysis of mRNA vaccines and,
146 in principle, could serve as a quality control step for mRNA therapeutics.

147

148 **Rapid deadenylation of mRNA-1273 in model cell lines**

149 We then used eDRS to monitor stability and poly(A) tail status in cells typically used for pre-clinical
150 analysis. We first determined the optimal amount of vaccine RNA: non-toxic to cells, allows efficient
151 protein production, and detectable in bulk RNA with eDRS (**Fig. 2a**, ED Fig. 2ab). Then, HEK293T and
152 A549 cells were transfected and cultured for up to 72 h, followed by RNA extraction and DRS. eDRS
153 efficiently separated vaccine mRNA from endogenous mRNAs (ED Fig. 2c), allowing recovery of up to
154 twice as many reads, compared to the standard basecalling/mapping (ED Fig. 2d). Analysis of poly(A) tails
155 revealed that m^ΨCm^ΨAG was swiftly removed in both cell lines, followed by deadenylation (**Fig. 2bc**, ED
156 Fig. 2e); this was observed as a reduction in mean poly(A) length with time, accompanied by a decreased
157 number of vaccines reads. Concordantly with the RNA decay, spike protein levels also decreased with time
158 (**Fig. 2d**), confirming direct relation between RNA stability and protein production.

159 To verify the role of deadenylation in mRNA-1273 decay, we constructed a HEK293T line with
160 tetracycline-inducible depletion of the scaffold subunit (CNOT1) of the primary deadenylase complex
161 CCR4-NOT. CNOT1 depletion increased global poly(A) lengths of endogenous mRNAs (ED Fig. 2f) and
162 also decreased poly(A) tail shortening in mRNA-1273, compared to the uninduced state (**Fig. 2e**). We only
163 observed significant changes in poly(A) length in reads lacking the terminal m^ΨCm^ΨAG pentamer. The
164 ratio of transcripts lacking the pentamer remained the same in both conditions, implying that CCR4-NOT
165 is not involved in pentamer removal. These observations indicate that, as previously suggested based on
166 the analysis of endogenous transcripts, deadenylation limits the lifetime of therapeutic mRNAs in model
167 cell lines.

168

169 **Re-adenylation of mRNA-1273 *in vivo***

170 The exact fate of mRNA therapeutics depends on many factors, which are hard to recapitulate in model cell
171 lines. The micro-environment at the site of RNA delivery and the gene expression patterns specific to cells

172 taking up the mRNA may influence its stability and, thus, the therapeutic outcome. Hence, we
173 intramuscularly delivered mRNA-1273 via an *in vivo* mouse model to study vaccine mRNA metabolism.
174 We isolated RNA from the tissues at the injection sites 2, 8, and 24 h post-immunization (**Fig. 3a**) and
175 observed that vaccine mRNA quickly diminishes from the injection site and is barely detectable after 24 h
176 (**Fig. 3b**). eDRS was conducted for samples where a sufficient amount of vaccine mRNA was detected (as
177 revealed by qPCR). Of interest, the majority of mRNA-1273 poly(A) tails contained mΨCmΨAG 24 h after
178 injection, though mild deadenylation of processed tails was noticeable at all analyzed time points (**Fig. 3c**).
179 To our surprise, a substantial fraction of mRNA-1273 reads had increased poly(A) length, reaching up to
180 150-200As. All of these reads lacked the terminal pentamer, suggesting that re-adenylation of vaccine RNA
181 occurs after its removal. At this juncture, most of the injected vaccine RNA would have been taken up by
182 immune cells and transferred to draining lymph nodes⁶. Unfortunately, due to the overall low prevalence
183 of mRNA-1273 in lymph nodes, compared to injection sites⁶, we could not analyze similar poly(A) tail
184 extension dynamics there.

185 To see whether mRNA-1273 re-adenylation occurs in monocyte/macrophages and DCs, which are reported
186 to be the major cell type taking up BNT162b2⁵, we analyzed vaccine metabolism using eDRS in *in vitro*
187 cultures of bone marrow-derived macrophages (BMDMs) and bone marrow-derived dendritic cells
188 (BMDCs, further termed DCs). Both types of cells were efficiently transfected mRNA-1273 LNPs without
189 visible toxic effects (ED Fig. 3a), allowing antigen translation for up to 72 h (**Fig. 3d**). Vaccine mRNA was
190 stable and easily detectable for at least 72 h, with around 25% of molecules having an intact 3' end after 4
191 h (**Fig. 3ef**, ED Fig. 3bc). We observed that 24 h after transfection, the poly(A) tails of vaccine mRNAs
192 were elongated by ~20As on average, reaching up to 200As in BMDMs (**Fig. 3e**, ED Fig. 3b). The mean
193 poly(A) length returned to the initial ~100As 72 h after transfection. Notably, dynamic change in
194 polyadenylation was observed only for tails lacking the 3' terminal pentamer, and mRNA-1273 reads with
195 an intact 3' end had, on average, the same length of poly(A) at all analyzed time points. Re-adenylation
196 was not observed in DCs (**Fig. 3f**, ED Fig. 3c).

197 In sum, our data show that mRNA-based vaccines can be stable and even undergo poly(A) tail elongation
198 *in vivo*, a novel result that has not previously been reported or considered in the literature.

199

200 **Global transcriptomic responses upon mRNA-1273 administration and induction of TENT5 poly(A)** 201 **polymerases**

202 Gene expression analysis of RNA samples isolated from injection sites revealed complex transcriptomic
203 responses following vaccination. Changes are already visible 8 h post-vaccination, with 1,129 genes
204 downregulated and 2,502 genes upregulated at 24 h, clustered into 3 groups (**Fig. 4a**, Supplementary Table
205 1). Examination of upregulated genes (clusters 2 and 3) revealed significant enrichment in functions related
206 to immune response and cell activation (**Fig. 4a**, ED Figure 4a, Supplementary Table 2). In addition, the
207 expression of genes related to basic metabolic processes was decreased (**Fig. 4a**, cluster 1, ED Fig. 4a,
208 Supplementary Table 1, Supplementary Table 2).

209 Patterns of gene expression following mRNA-1273 administration in BMDM cultures were similar to those
210 of transcriptomic responses at injection sites. 584 transcripts changed their expression, with the most
211 pronounced transcriptome reconstruction observed 24 h after vaccine administration and persistent till the
212 end of the experiment (72 h) (**Fig. 4b**, Supplementary Table 3). Those transcripts were clustered into 4
213 groups (**Fig. 4b**), two of which contained genes upregulated after 24 h and mainly associated with antigen
214 presentation (MHC components in cluster 1), innate immunity (*ApoE*, *Lyz2*, *CtsH*, *CtsS*) and interferon
215 induction (*Stat1*, *Mx1*, and multiple other *Ifi* transcripts) (**Fig 4b**, ED Fig. 4b, Supplementary Table 3,
216 Supplementary Table 4). These changes resemble responses previously reported for the BioNTech mRNA
217 anti-COVID19 vaccine (BNT162b2)⁵.

218 Intriguingly, in contrast to mRNA-1273 administration in BMDM cultures, almost no global changes in
219 transcription were observed in DCs, where only certain innate immunity effectors (*Ctsb*, *Ctsd*) and serum
220 complement element C1q (*Clqb*) were induced 72 h post administration (ED Fig. 4c, Supplementary Table
221 5).

222 As the vaccine mRNA is not expected to enter the nucleus, there should be a specific cytoplasmic
223 mechanism causing the extension of vaccine poly(A) tails after delivery to macrophages. Whole-
224 transcriptome poly(A) profiling revealed that the change in poly(A) length is not specific to mRNA-1273:
225 the poly(A) tails of 124 endogenous transcripts were significantly changed after treatment with mRNA-
226 1273 (Kruskall-Wallis test, $p < 0.001$), with immune-response-associated transcripts exhibiting the most
227 pronounced tail extension (average: 20As at 24 h, **Fig. 4c**; ED Fig. 4d, clusters 1 and 2; Supplementary
228 Table 6, Supplementary Table 7). They included MHC components (*H2-K1*, *H2-D1*, *H2-T23*, *B2m*), serum
229 complement components (*C1qb*, *C1qc*), lysosomal proteins (*Lamp1*, *Laptm5*), and innate immune response
230 genes (*Ctsb*, *Ctsd*, *ApoE*, *Lyz2*, *Cst3*, *Ctss*). Remarkably, in our previous study on BMDMs activated with
231 LPS²⁶, a similar set of transcripts was revealed to be substrates of TENT5A/TENT5C non-canonical
232 poly(A) polymerases. Therefore, we examined gene expression changes of all known non-canonical
233 poly(A)/poly(U) polymerases and found that *Tent5a* is the only polymerase that is significantly induced at
234 vaccine injection sites and after vaccine treatment in BMDMs (**Fig. 4d**, ED Fig. 4e). *Tent5c* is also
235 expressed but at a much lower level. At the same time, no change in the expression of subunits of
236 deadenylase complexes was observed (**Fig. 4e**). In contrast to BMDMs, both *Tent5a* and *Tent5c* were barely
237 expressed in DCs. These experiments suggest a possible role for TENT5A and, to a lesser extent TENT5C,
238 in the re-adenylation of mRNA-1273 that is observed in BMDMs, but not in DCs.

239

240 **mRNA-1273 polyadenylation by TENT5s is essential for the efficient production of spike protein and** 241 **immune response**

242 To evaluate the role of TENT5 proteins in vaccine mRNA re-adenylation, we studied mRNA-1273
243 metabolism in BMDMs devoid of TENT5A and TENT5C (double-knockout *Tent5a*^{Flox/Flox}/*Tent5c*^{-/-})²⁶.
244 Double-knockout BMDM cells were treated with mRNA-1273 for up to 72 h, RNA was isolated and
245 subjected to eDRS. In comparison to BMDM WT cells, we observed relatively fast mRNA-1273 decay and
246 deadenylation in the absence of TENT5A and 5C (**Fig. 5a**, SD Fig. 5a), with mean poly(A) tails shortened

247 to 80As after 24 h, despite the high ratio of RNAs lacking the 3' pentamer. This indicates a critical role of
248 TENT5A/C proteins in the regulation of mRNA-1273. Indeed, in *Tent5a^{Flox/Flox}/Tent5c^{-/-}* BMDMs stability
249 of mRNA-1273 is drastically reduced (**Fig. 5c**).

250 TENT5A/C also affected endogenous transcripts as no extension of poly(A) tails following vaccination was
251 observed for mRNAs noticed in WT (ED Fig. 5b, Supplementary Table 6), including innate immunity
252 effector transcripts (clusters 1,2), previously observed in LPS-activated macrophages²⁶. Importantly,
253 dysfunction of TENT5-mediated cytoplasmic polyadenylation did not affect the transcriptional response,
254 which was similar for both WT and *Tent5a^{Flox/Flox}/Tent5c* BMDMs (ED Fig. 5c, Supplementary Table 8).

255 Most mRNAs with poly(A) tails elongated after vaccination in WT BMDMs, but not *Tent5a^{Flox/Flox}/Tent5c^{-/-}*
256 *BMDMs*, (ED Fig. 5b) encode extracellular proteins translated at the endoplasmic reticulum (ER), in line
257 with previous findings regarding TENT5A/C substrates^{26,27}. Notably, mRNA-1273 also encodes an ER-
258 targeted protein, which, as we show, hijacks TENT5s to extend its poly(A) tail. To confirm the specificity
259 of TENT5A to mRNAs encoding proteins traversing the ER, we co-transfected WT BMDMs with purified
260 mRNA-1273 RNA and firefly luciferase-encoding mRNA reporter (mΨ containing *in vitro* transcribed
261 mRNA, with ~75As tail). After 24 h, we collected RNA for eDRS. The elongation of poly(A) tails was
262 observed for mRNA-1273, but not for the luciferase reporter, which is not translated on the ER (ED Fig.
263 5de). Curiously, the poly(A) tail elongation of mRNA-1723 was even more pronounced than in previous
264 experiments, possibly because of increased availability of mRNA to the polyadenylation machinery, as
265 compared to LNP-based delivery.

266 DCs are major antigen-presenting cells and are expected to play a major role in immunity development
267 after vaccination. However, DCs express low levels of TENT5, raising the question of whether TENT5-
268 mediated stabilization of vaccine mRNA in macrophages affects immune response. TENT5C is expressed
269 in B cells, and was shown to regulate the humoral response by polyadenylation of immunoglobulin
270 transcripts²⁸, whereas TENT5A was described only in the context of innate immunity²⁶. Thus, we
271 immunized WT and *Tent5a^{-/-}* mice with mRNA-1273, and measured antigen and antibody production (**Fig.**

272 **5d**). Significantly lower spike (S) protein concentrations were observed in *Tent5a*^{-/-} mouse serum, both at
273 days 2 and 4 post-immunization, compared to WT (**Fig. 5e**). Further, the S protein concentration was
274 significantly decreased on day 4, compared to day 2 (ED Fig. 5f). Thus, mRNA-1273 stabilization through
275 TENT5A-mediated re-adenylation has a direct effect on antigen production, both the amount and the
276 longitude. However, some effects on macrophage secretory capability caused by *Tent5a* KO can also
277 contribute to decreased levels of the antigen. Importantly, the level of serum anti-spike IgG 14 days post-
278 immunization was significantly lower in *Tent5a*^{-/-}, and in 3 of 4 mice was barely detectable (**Fig. 5f**), despite
279 the overall higher level of IgGs in the sera compared to WT animals (ED Fig. 5g). These data indicate that
280 impaired immune response in *Tent5a*^{-/-} animals is directly related to diminished antigen translation and
281 subsequent presentation. Moreover, since a good correlation exists between the S protein concentration in
282 serum and spike-specific IgG in immunized mice (**Fig. 5g**), we postulate that secretion of the antigen by
283 macrophages after intramuscular administration of mRNA vaccines plays a significant role in building the
284 immune response.

285 Overall, our results indicate that mRNA vaccine metabolism varies across cell types and that this has a
286 significant influence on immunization efficacy.

287

288 **Discussion**

289 The Covid-19 pandemic accelerated vaccine technology development, and the timely introduction of
290 mRNA vaccines has played an essential role in slowing the spread of the disease-causing virus, SARS-
291 CoV-2. This report provides the first evidence that therapeutic mRNAs are modified in cells, such that their
292 poly(A) tails are extended by the cellular machinery. We also demonstrate that cellular mRNA processing
293 varies between cell types and tissues. Here, we identify TENT5A cytoplasmic poly(A) polymerase as
294 responsible for vaccine mRNA re-adenylation, and we show that re-adenylation enhances the stability of
295 mRNA therapeutics in macrophages and affects the magnitude of the humoral immune response. Finally,
296 we implement a highly efficient methodology based on direct RNA sequencing (DRS) for the analysis of

297 mRNA therapeutics. Together, our results offer an explanation for the efficacy of existing mRNA vaccines
298 and may profoundly influence the development of next-generation mRNA therapeutics.

299 After administration, mRNA vaccines build immune responses in a complex way. Before COVID-19,
300 efforts related to mRNA vaccine development were primarily focused on developing anti-cancer agents^{11,29}.

301 Although mRNA design was usually optimized in cell lines, the aim was to target dendritic cells that are
302 assumed to produce and present the antigen, to build both humoral and cellular adaptive immune responses.

303 Here, for the first time, we show that macrophages play a critical role and are responsible for antigen
304 production. Not only are monocytes/macrophages the major cell populations that take up vaccine mRNA^{5,9},

305 but these cells also express TENT5A, which re-adenylates mRNA-1273, thereby increasing its stability and
306 protein output. In *Tent5a*^{-/-} mutant mice, a significant drop in antigen production is observed, coinciding

307 with the impaired development of an antigen-specific humoral response. Thus, it can be expected that spike
308 (S) proteins produced by macrophages, either at the site of vaccine inoculation or in the draining lymph

309 nodes (where LNPs are transported and captured by macrophages), are endocytosed by LN resident DCs,
310 resulting in induction of Th1 and Tfh cells, and follicular DCs, resulting in induction of humoral immune

311 response.

312 Although the data presented were obtained using mRNA-1273, similarity in the mode of action of
313 BNT162b2 indicates a likely role for TENT5A for this vaccine as well. Moreover, the fact that TENT5

314 substrates must be terminated with poly(A) sheds new light on the different efficacies of two anti-COVID19
315 mRNA vaccine prototypes developed by CureVac (CV). The original prototype, which failed clinical trials

316 due to low efficacy, had a heavily engineered 3' end: its poly(A)₆₄ was followed by poly(C)₃₀ and a histone
317 stem-loop^{16,30}. In contrast, the second generation prototype, CV2nCoV, which was more potent in building

318 immune response, terminates with a poly(A) tail¹⁶ and thus would be amenable for TENT5 mediated re-
319 adenylation.

320 Development of therapeutic mRNAs goes beyond vaccines, and intensive efforts are underway to use
321 mRNA to treat many mendelian diseases or induce the production of therapeutic proteins. In these cases,

322 the main target is the liver, as the transfection of hepatocytes is very efficient after intravenous delivery of
323 LNP-encapsulated mRNAs. There are also attempts to target other organs/cell types. Here, we show that
324 various cell types metabolize mRNA vaccines differently. Only those expressing high levels of TENT5s
325 would be expected to stabilize mRNA through re-adenylation. Although the mechanism of substrate
326 recognition by TENT5 is largely unknown, ER targeting is a prerequisite feature (**Fig. 5c**). Further
327 mechanistic research will be needed to decipher substrate recognition of TENT5 poly(A) polymerases and
328 to explore their physiological roles. However, it is clear that target cells expressing high levels of TENT5s
329 will be desirable for therapeutic mRNAs encoding secreted proteins. Moreover, better knowledge about
330 substrate recognition will allow for the rational design of mRNAs much more efficiently polyadenylated
331 by TENT5 and, therefore, more stable. Other tissue-specific mechanisms of mRNA stabilization may also
332 be uncovered in the future. All these observations emphasize that the design of therapeutic mRNAs needs
333 to be tailored to the target cells and the target site of the protein product.

334

335

Methods

336

337 Mice lines and immunization

338 All mice lines were generated by the CRISPR/Cas9-based method in the Genome Engineering Unit
339 (<https://crisprmic.eu/>) as described in ref. ^{24,25,30}. A double knockout *Tent5a^{Flox/Flox}/Tent5c^{-/-}* was described
340 previously²⁶. Mice were bred in the animal house of the Faculty of Biology, University of Warsaw, and
341 maintained under conventional conditions^{24,25,30} in open polypropylene cages filled with wood chip bedding
342 enriched with nest material and paper tubes. Mice were fed ad libitum with a standard laboratory diet
343 (Labofeed B, Morawski). Humidity in the rooms was kept at 55 ± 10%, the temperature at 22 °C ± 2 °C, at
344 least 15 air changes per hour, and the light regime set at 12 h/12 h (lights on from 6:00 to 18:00). Health
345 monitoring was performed regularly at the IDEXX laboratory.

346 Discarded remnant vaccination material (Moderna mRNA-1273, Spikevax) was used within
347 manufacturer's guidelines for stability. Because this was not available for purchase and as only remnant
348 (otherwise to be discarded) material could be used at the time, we obtained approval from the Polish
349 Ministry of Health (MMI.454.1.2021.TM).

350 Mice were immunized by intramuscular (*Vastus lateralis* region) injection either with 25µl of 0.9% NaCl
351 (controls) or 25µl of Moderna's mRNA-1273 at 40 ng/µl concentration. Tissues were collected after 2, 8
352 and 24 hours post-injection and snap-frozen in liquid nitrogen. Serum was collected at day 2, 4 and 14 after
353 immunization. All animal experiments were approved by the II Local Ethical Committee in Warsaw
354 affiliated with the University of Warsaw, Faculty of Biology (approval numbers: WAW2/71/2021,
355 WAW2/129/2021, WAW2/95/2022)) and were performed according to Polish Law (Act number 653
356 266/15.01.2015) and in agreement with the corresponding European Union directive.

357 ELISA

358 The concentrations of spike protein, anti-spike IgG and total mouse IgG in mice serum were measured with
359 commercially available ELISA kits: Sinobiological (#KIT40591), Eagle Bioscience (#KBVH015-14) and
360 (#OGG11-K01) respectively. All reactions were conducted according to the manufacturer's
361 recommendation.

362 **Cell cultures**

363 A549 and HEK293 Flp-In T-REx cell lines and its derivate's were cultured in Dulbecco's modified Eagle's
364 medium (DMEM; Gibco) supplemented with 10% FBS (Gibco) and penicillin/streptomycin (Sigma-
365 Aldrich) at 37°C in a 5% CO₂ atmosphere until 80% confluency. To produce the HEK293 Flp-In T-REx
366 cells (R78007, Thermo Fisher Scientific) cell line with conditional knock-down of CNOT1 we designed a
367 tri-miRNA construct (listed below; stem-loop sequences ATGGAAGAGCTTGGATTTGAT;
368 CTCCCTCAATTCGCCAACTTA; AGGACTTGAAGGCCTTGTCAA), which was cloned at the BspTI
369 (AflII) + NotI restriction sites in a pKK-RNAi vector (pKK-BI16 nucCherry EGFP-TEV³¹), which is a
370 derivative of the pcDNA5/FRT/TO vector. 1 mln HEK293 Flp-In T-REx cells were grown on DMEM High
371 glucose (Gibco) supplemented with 10% fetal bovine serum on 6-well plates. To transfect cells 300 ng of
372 the miCNOT1 bearing construct was mixed with 1 µg of pOG44 plasmid, 250 µl of OptiMEM media and
373 supplemented with 2 µl TransIT-2020 Transfection Reagent (Mirus, MIR5400). The transfection mix was
374 incubated 20 min at room temperature and then added to the cell culture for 24 h. Then cells were transferred
375 to a 60 mm plate and cultured in a DMEM high glucose media supplemented with 40µg/ml hygromycin
376 and 8 µg/ml blasticidin for the first 6-7 days and then the media was replaced with media of increasing
377 antibiotic concentration to 50 µg/ml hygromycin and 10 µg/ml blasticidin. Cells were grown until single
378 colonies appeared 4 weeks later. A control of cells non-transfected with the pKK-BI16 plasmid was
379 included to ensure the specific selection of the cell line.

380 Expression of exogenous miRNA genes was induced by the addition of doxycycline (Thermo Fisher
381 Scientific) at a final concentration of 100 ng/ml. Cell enumeration was performed by crystal violet (Sigma,
382 C3886) staining described by Xin Chen Lab (UCSF).

383 **Murine bone marrow-derived macrophages (BMDM) cell cultures**

384 The primary BMDM cell cultures were established from the bone marrow monocytes isolated from
385 *Tent5a*^{Flox/Flox}/*Tent5c*^{-/-} and wild-type mice. Young adult mice (12-25 weeks old) were sacrificed by cervical
386 dislocation, then femurs and tibias were isolated and bone marrow was harvested by centrifugation-based
387 protocol^{32,33}. Bone marrow cells were plated in IMDM medium (Thermo Fisher Scientific; 21980065)
388 supplemented with 10% FBS (Gibco), 100 U/ml penicillin/0.1 mg/ml streptomycin solution (Sigma-
389 Aldrich), and 10 ng/ml macrophage colony-stimulating factor (M-CSF, Preprotech; 315-02) and cultured
390 at 37 °C in 5% CO₂. For conditional *Tent5a* gene targeting, BMDM cells were transduced on the 8th day
391 after isolation with lentivirus carrying Cre recombinase (pCAG-Cre-IRES2-GFP). The lentivirus
392 production, cell transduction and genotyping were performed as described previously^{26,28}. Cells were used
393 for experiments on the 14th day after isolation.

394 **Murine bone marrow-derived dendritic cells (BMDCs) isolation and culture**

395 Bone marrow was flushed with cold PBS from the femurs of 6-week-old female C57BL/6 mice. RBCs were
396 lysed using ACK (Ammonium-Chloride Potassium) Lysing Buffer (ThermoFisher Scientific) according to
397 the manufacturer's protocol. All the remaining cells were suspended at 1 x 10⁶/ml density in the culture
398 medium [RPMI 1640 medium (Sigma-Aldrich) supplemented with heat-inactivated 10% (v/v) fetal bovine
399 serum (HyClone), 2 mM L-glutamine (Sigma-Aldrich), 100 U/ml penicillin and 100 µg/ml streptomycin
400 (both from Sigma-Aldrich)], plated at ø10 cm non tissue culture-treated Petri dishes (Sarstedt) and placed
401 at 37 °C in the atmosphere of 5% CO₂ in the air. Differentiation towards DCs was induced with 200 ng/ ml
402 recombinant murine FLT3L (Peprotech). On day 7th 600 pg/ml of recombinant murine GM-CSF
403 (Peprotech; 315-03) was added for 4-day incubation. On day 11th loosely adherent and floating cells were
404 collected for subsequent experiments.

405 **mRNA-1273 administration to in vitro cultured cells**

406 The 0.5-1M cells were seeded day before on 6-well plate in media as described above. 5 µl of mRNA-1273
407 (200 ng/µl) were diluted in 150 µl of Opti MEM media (Thermo Fisher Scientific), at room temperature

408 and after 10 min. added to the cells in drop-wise manner and gently mixed. Cells were harvested at time
409 points specified for the individual experiments.

410 The mRNA transfections, using purified mRNA-1273 and FLuc spike-in, were carried out with
411 Lipofectamine MessengerMAX (Thermo Fisher Scientific), according to manufacturer's instructions. Cells
412 were harvested 24 h after transfection for subsequent analyses.

413 **General molecular biology techniques**

414 *Western blots*

415 An equal number of cells were lysed in PBS supplemented with 0.1% NP40, protease inhibitors and
416 viscolase (final concentration 0.1 U/ml; A&A Biotechnology, 1010-100) for 30 min at 37 °C with shaking
417 1200 rpm, then 3x SDS Sample buffer (187.5 mM Tris-HCl pH 6.8, 6% SDS, 150 mM DTT, 0.02%
418 Bromophenol blue, 30% glycerol, 3% 2-Mercaptoethanol) was added and samples were boiled for 10 min.
419 Samples were resolved on 12–15% SDS–PAGE gels and then proteins were wet transferred to Protran
420 nitrocellulose membranes (GE Healthcare) at 400 mA at 4 °C for 1.5 h in 1x Transfer buffer (25 mM Tris
421 base, 192 mM glycine, 20% methanol (v/v)). Next, the proteins were visualized by staining with 0.3% w/v
422 Ponceau S in 3% v/v acetic acid and digitalized. Membranes were blocked by incubation in 5% milk in
423 TBST buffer for 1 h followed by overnight incubation at 4 °C with specific primary antibodies (listed in
424 Table 1) diluted 1:2500 (spike protein, firefly luciferase, and PDI) or 1:5000 (α -tubulin, β -actin, and
425 GAPDH). Membranes were washed three times in TBST buffer, 10 min each, incubated with HRP-
426 conjugated secondary antibodies: anti-mouse (Millipore, 401215) diluted 1:5000 and anti-rabbit (Millipore,
427 401393) diluted 1:5000, for 2 h at room temperature. Membranes were washed three times in TBST buffer
428 and proteins were visualized using ChemiDoc System (BioRad) or X-ray films. Unprocessed scans of
429 selected major blots and gels are shown in the Extended Data Fig. 6.

430 Antibodies used in this study are listed in Table 1 below

431 *Table 1 Antibodies used in this study*

Antibodies	Manufacturer and catalog number
Anti-SARS-CoV-2 Spike Glycoprotein S1 antibody	Abcam, ab275759
Anti-Firefly Luciferase	Abcam; ab21176
Anti-GAPDH	Novus Biologicals, NB300-327
Anti-Tubulin	mAb (DM1A), CP06
Anti-Actin	Cell Signaling; 2146
Anti-PDI (C81H6)	Cell Signaling; 3501
Goat Anti-Mouse IgG, H&L Chain Specific Peroxidase Conjugate	Millipore Cat# 401215
Goat Anti-Rabbit IgG, H&L Chain Antibody, Peroxidase Conjugated	Millipore Cat # 401393

432

433 *RNA isolations*

434 Total RNA was isolated from cells or vaccine samples with TRIzol reagent or TRIzolTMLS Reagent (both
435 from Thermo Fisher Scientific), respectively, according to the manufacturer's instructions, dissolved in
436 nuclease-free water and stored at -20 °C (short term) or -80 °C (long term). RNA from frozen muscles and
437 lymph nodes were isolated by tissue homogenization in TRI-reagent (Sigma, T9424) pre-heated to 60 °C,
438 using Omni Tissue Homogenizer (TH) equipped with 7 x 115 mm Saw Tooth (Fine) Generator Probe,
439 homogenous mixtures were further processed according to the manufacturer's instructions. For RT-qPCR,
440 RNA-seq and DRS library preparation, the RNA was treated with TURBO DNase (Thermo Fisher
441 Scientific; AM1907; or InvitrogenTM, AM2238). To assess the integrity of the used material, each RNA
442 sample after DNase treatment was analyzed with Agilent 2200 TapeStation system, using Agilent High
443 Sensitivity RNA ScreenTape (Agilent, 5067-5579).

444 **mRNA-1273 quantification**

445 cDNA was synthesized using 500 ng of DNAsed total RNA as template with SuperScriptTM III Reverse
446 Transcriptase (InvitrogenTM, 18080093) according to manufacturer's instructions. Final cDNA
447 concentration was kept at 2,5 ng/ul (converted from total RNA).

448 For assessment of Moderna's mRNA-1273 concentration in mouse tissues, custom made TaqMan probe
449 was used together with TaqMan™ Gene Expression Master Mix (Applied Biosystems™, 4369016). Pre-
450 designed gene expression assay for beta-Actin (Applied Biosystems™, Mm01205647_g1) was used for
451 normalization. The reaction mix was contained in 10 µl total volume with 1x concentration of master mix
452 and gene expression assay, 5 ng cDNA was used per reaction (converted from total RNA). Thermal cycling
453 program for TaqMan™ Gene Expression Master Mix was used as instructed by the manufacturer.

454 For relative gene expression estimation of *Tent5a* and *Tent5c* at injection sites, and mRNA-1273 levels in
455 HEK293T and A549 cells with varying amounts of vaccine, we used Platinum™ SYBR™ Green qPCR
456 SuperMix-UDG (Invitrogen™, 11733046) following the general protocol for ABI instruments
457 recommended by the manufacturer.

458 QuantStudio™ 5 Real-Time PCR System, 384-well (Applied Biosystems™, A28140) was used in case of
459 all RT-qPCR analyses.

460 *Custom TaqMan probe design*

461 Primer blast algorithm was used to find a unique amplicon for mRNA-1273 within mouse transcriptome
462 (Refseq mRNA). Within the amplified region, a 15-mer of optimal GC content (53,3%) was selected as
463 target site for probe hybridization. We selected FAM dye and MGB-NFQ quencher as 5' and 3'
464 modifications for the probe. The probe was synthesized by ThermoFisher's Custom TaqMan® Probes
465 service. In order to test the specificity and sensitivity of designed assay we performed a serial dilution
466 experiment in which we spiked 500 ng of DNAsed murine total RNA with 50 ng of DNAsed mRNA-1273
467 and performed cDNA synthesis. Then we performed 10x serial dilutions of said mix with unspiked murine
468 cDNA of the same concentration. RT-qPCR analysis has shown that the designed assay is specific and can
469 detect up to 10 ag of mRNA-1273 per ng of total RNA which is equivalent of roughly 25 molecules.

470 Primers and probe sequences as well as working concentrations were as listed in Table 2 below:

471 *Table 2 Primers and probe sequences*

Name	Sequence 5'-3'
TaqMan VacProbe2	CACCAAGCTGAACGA
TaqVac Fw	GATCAGCAACTGCGTGG
TaqVac Rv	TACACGTTGGTGAAGCAC
Act_F	CCCAGATCATGTTTGAGACC
Act_R	ATCACAATGCCTGTGGTACG
Vac5_fw	CACCTTCAAGTGCTACGG
Vac5_rv	TAGTTGTAGTCGGCGATCTT
Gapdh_F	AAGGGCTCATGACCACAGTC
Gapdh_R	GATGACCTTGCCACAG
Teng5a_F	GCTCACTCTCAAGGAGGCTTATG
Tent5a_R	CTTCAGCTCCACATTTTTGCCAC
Tent5c_F	CAGTCACCTCCTCTTCCAACG
Tent5c_R	AACCTGATCCCAGTTGAGCAC

472

473 **3'RACE-seq**

474 To examine 3'UTR and terminal sequence of the mRNA-1273, RNA was freshly isolated from the vaccine
475 sample vial. Then 1 µg of vaccine mRNA was ligated to 20 pmols RA3_7N adaptor:
476 5rApp/CTGACNNNNNNNTGGAATTCTCGGGTGCCAAGG/3ddC with 10U of T4 KQ227 RNA ligase
477 1 (#M0204S NEB) in the presence of 20U RNase OUT (#10777019, Thermo Fisher Scientific), 1x T4 RNA
478 Ligase Reaction Buffer (#M0204S NEB), 1mM ATP, 20% PEG8000 in total 20 µl reaction volume at 25 °C

479 for 4 h. Ligase was inactivated at 65 °C for 20 min. The ligation product was purified with 0.8x ratio KAPA
480 Pure Beads and eluted with 15 µl RNase-free water, according to manufacturer protocol. The cleaned
481 ligation product was subjected to reverse transcription with 40 pmol of Illumina index adapter:
482 5'CAAGCAGAAGACGGCATAACGAGATATCAGTGTGACTGGAGTTCCTTGGCACCCGAGAATT
483 CCA3' with SuperScript III (#18080093, Thermo Fisher Scientific), 1x First Strand Buffer (#18080093,
484 ThermoFisher), 0.25mM dNTP mix, 5mM DTT, 20U RNase OUT (#10777019, Thermo Fisher Scientific).
485 The reaction mix was incubated at 45 °C for 1 hour and 70 °C for 20 min in a thermocycler. Reverse
486 transcription product was cleaned with 1x ratio KAPA Pure Beads and eluted with 19 µl RNase-free water.
487 Prepared cDNA was diluted in 1:3 proportion. In the library amplification step, 0.5 µl of cDNA was mixed
488 with 0.4 pmol of gene-specific starter
489 5'AATGATACGGCGACCACCGAGATCTACACGTTTCAGAGTTCTACAGTCCGACGATCAGAAG
490 GAGATCGATCGGCTG3', 0.2 pmol of RP universal starter
491 5'CAAGCAGAAGACGGCATAACGAGAT3', 0.25mM dNTP, Phusion High-Fidelity DNA Polymerase
492 (#F530S, Thermo Fisher Scientific), 1x Phusion HF Buffer (#F530S, ThermoFisher), 3% DMSO. For
493 amplification, a standard Phusion program was used with 65 °C for annealing and 25 cycles. The 50 µl of
494 PCR product was separated in 2.5% agarose gel. A band of 450bp was cut out from the gel and purified
495 with Gel-OUT (#023-50, A&A Biotechnology) according to the kit protocol. The library was cleaned twice
496 with 1.0x ratio of KAPA Pure Beads. TapeStation analysis of the sample was performed as quality control.
497 The library was sequenced on Illumina NovaSeq 6000 sequencer.

498 **3'-RACE-seq data analysis**

499 RA37_N adapter sequence was trimmed from the R2 read (containing poly(A) tail) with cutadapt³⁴ (options
500 -g CCTTGGCACCCGAGAATTCCANNNNNNGTCAG --discard-untrimmed). Then only reads
501 containing poly(A) tail were identified with cutadapt (options -a TTTTTT --discard-untrimmed --fasta).
502 Obtained sequences were reverse complemented using fastx_reverse_complement from the fastx toolkit
503 (0.0.13) and loaded into R with BioStrings package. To get rid of unwanted trimming artifacts sequences

504 with length between 0 and 10 were chosen, four A letters (representing poly(A) tail) were pasted before
505 each sequence for visualization purposes, and sequence logo representing nucleotide composition of 3' end
506 of mRNA-1273 was produced with ggseqlogo package³⁴.

507 **Preparation of standards with predefined poly(A) lengths**

508 Spike-ins RNA were *in vitro* transcribed from a set of double-stranded DNA fragments. Templates for
509 transcription were prepared in two consecutive PCR reactions. First, a desired fragment of Renilla luciferase
510 from pRL5Box plasmid was amplified using RLuc_F1/R1 specific primers containing an overhang
511 common for all primers utilized in the second round of PCR (Table 3). PCR products were verified through
512 gel electrophoresis. Correct amplicons were used as templates in the second PCR reaction with
513 RLuc_T7_F2 primer, hybridizing to the overhang sequence from RLuc_F1 and containing the T7 promoter,
514 and backward primer RLuc_Ax_R2, hybridizing to the overhang sequence from RLuc_R1 oligo and
515 introducing poly(A) tail of a defined length (from 10 to 120 As). Resulting PCR products were assessed
516 and purified by gel electrophoresis. *In vitro* transcription reaction was performed at 37 °C for 1.5 h in a 50
517 µl reaction volume containing: 600 pmols T7 template, 10 µl of 5x transcription buffer (200mM Tris-HCl,
518 30mM MgCl₂, 10mM spermidine, 50mM NaCl), 5 µl of rNTPs mix (20mM each), 5 µl of 100mM DTT,
519 0.5 µl of 1% Triton X-100, 80U Ribonuclease Inhibitor, 100U T7 RNA polymerase. Then, DNA template
520 was removed with TURBO DNase (Ambion) for next 15min. Spike-ins RNA were phenol/chlorophorm
521 extracted, precipitated, visually assessed by denaturing electrophoresis, purified on RNA purification beads
522 and subjected as controls in DRS runs. In each DRS run, a mixture of spike-ins representing RNAs with
523 poly(A) tail of defined length:A10/ A15/ A30/ A45/ A60/ A90/ A120 was included.

524

525 *Table 3 Primers used for spike-ins preparation*

Name	Sequence
RLucF1	5'-gccatcagattgtgtttgttagtcgctATGATTCCGAGAAGCACGCCGAGAAC3'

538 digested with 7U of DNase I (Thermo Fisher Scientific) for 30 min at 37 °C. To stop the reaction, 8 µl of
539 500mM aqueous Na₂EDTA solution was added. The crude RNA was purified using POROS™ Oligo
540 (dT)₂₅ Affinity Resin (Thermo Fisher Scientific) according to the manufacturer's protocol. The mRNA
541 was condensed to 100 µl volume using the Amicon® Ultra-4 centrifugal filter (Milipore) and finally
542 purified using HPLC and the RNASep™ Prep column (ADS Biotec), using the following conditions: eluent
543 A -100mM TEAAc, eluent B - 200mM TEAAc/ACN; 10–35% of eluent B in 32 min, precipitated as sodium
544 salt (3M NaOAc pH 5.2, isopropanol/ 80% EtOH) and dissolved in water. The concentration of mRNA was
545 determined using absorbance measurements. To check the purity of the mRNA preparations, 100 ng of
546 mRNA was applied to 1% agarose gel and electrophoresis (20 min, 140 V) was performed.

547 **Inosine tailing and Nanopore DRS**

548 2 µg of RNA isolated from mRNA-1273 vaccine sample was denatured in the presence of 20U RNase
549 OUT (#10777019, ThermoFisher) at 65 °C for 3 min and immediately placed on ice. I-tailing reaction was
550 done with 0.5mM ITP (inosine triphosphate), 1x NEB 2.0 buffer (#B7002, NEB) and 2U of poly(U)
551 polymerase (#M0337S, NEB) at 37 °C for 45 min and terminated by snap-freeze in liquid nitrogen. I-tailed
552 RNA was cleaned twice on KAPA Pure Beads (#7983298001, Roche) in a 1x ratio and used for DRS library
553 preparation. I-tailed samples require ligation of special adaptor RTA_C10, which contains 10 cytosines at
554 the 3'end: 5' GAGGCGAGCGGTCAATTTTCCTAAGAGCAAGAAGAAGCCCCCCCCCCCC 3'. To
555 make the I-tailing specific RTA adaptor we followed ONT Direct RNA Sequencing - Sequence-
556 Specific protocol (Oxford Nanopore Technologies). 0.5 µg of I-tailed mRNA-1273 was taken to the first
557 ligation step of DRS library preparation. Library preparation was performed as given in ONT Direct
558 Sequencing protocol.

559 **Nanopore sequencing**

560 Direct RNA sequencing was performed as described by Bilaska et al., 2020²⁸. For raw vaccine isolate, 0.5
561 µg of RNA was used for the library preparation. For RNA isolates obtained from cell cultures or mouse
562 tissues, 3.5-5 µg of total mRNA was mixed with 50-200 ng oligo-(dT)₂₅-enriched mRNA from

563 *Saccharomyces cerevisiae* yeast and standards with predefined poly(A) lengths and processed with a Direct
564 RNA Sequencing Kit (catalog no. SQK-RNA002, Oxford Nanopore Technologies) according to the
565 manufacturer's instructions. Sequencing was performed using R9.4 flow cells on a MinION device (ONT).
566 Raw data were basecalled using Guppy (ONT). Raw sequencing data (fast5 files) were deposited at the
567 European Nucleotide Archive (ENA, project PRJEB53190).

568 **Identification of mRNA-1273-originating reads using subsequence Dynamic Time Warping**

569 For the comparisons of raw signals from nanopore sequencing, the DTAIDistance library³⁵ (version 2.3.5)
570 was used. Reference signal was obtained from one of the reads from the DRS run of crude mRNA-1273
571 material (read id: df408ab3-7418-4ee4-9a67-92743257b20a), which was giving good coverage of 3' end of
572 mRNA-1273 reference. The 5000 data points, covering part of poly(A) tail (1000 data points) and 3' end
573 of transcript (4000 data points) were selected for further processing (ED Fig. 1b). Such fragment of raw
574 current readout was smoothed using Savitzky-Golay filter (savgol_filter function from Scipy Python
575 library), with window length set to 51 and polynomial order set to 3, and normalized using zscore function
576 from stats python package. Raw sequencing data were read from fast5 files using ONT Fast5 API (version
577 4.0.0), first 20000 data points (which usually covers the 3' end of sequenced RNA) were selected, then
578 smoothed and normalized in the same way as reference signal. Then, the subsequence_alignment function
579 from DTAIDistance library was used to find a region in raw data with the best match to the reference signal.
580 As the output for each sequencing read the location of match and distance score, calculated using
581 distance_fast function from DTAIDistance library, was reported. The python script for all described
582 operations is available at https://github.com/LRB-IIMCB/DTW_mRNA-1273

583 **Poly(A) lengths determination and statistical analysis**

584 Basecalled nanopore reads were mapped to respective transcriptome reference using Minimap2 2.17 with
585 options -k 14 -ax map-ont --secondary=no and processed with samtools 1.9 to filter out supplementary
586 alignments and reads mapping to reverse strand (samtools view -b -F 2320). The poly(A) tail lengths for
587 each read were estimated using the Nanopolish 0.13.2 polya function²⁵.

588 For the analysis of mRNA-1273-originating reads the nanopolish polyA algorithm was modified to (1)
589 include unmapped reads, what allowed analysis of poly(A) lengths for sDTW-identified reads (2) detect
590 mΨCmΨAG at the 3' end of poly(A) tail and report its presence in the output.

591 For the detection of mΨCmΨAG the original segmentation algorithm was modified to include additional
592 segment between adaptor and poly(A), with mixed Gaussian distribution emissions, which were manually
593 estimated using MLE. As the result 4 additional columns are added to the nanopolish-polya output,
594 containing localization of mΨCmΨAG in the raw signal, its length, summed poly(A) + mΨCmΨAG length,
595 and information if mΨCmΨAG was detected. Detection of mΨCmΨAG is run with the nanopolish polyA-
596 moderna function. The source code of modified nanopolish is available at [https://github.com/LRB-](https://github.com/LRB-IIMCB/nanopolish_Moderna)
597 IIMCB/nanopolish_Moderna .

598 P values for each transcript were estimated using the Kruskal-Wallis test and adjusted for multiple
599 comparisons using the Benjamini–Hochberg method. Transcripts were considered as having a significant
600 change in poly(A) tail length, if the adjusted P value was < 0.05, and there were at least 20 supporting reads
601 for each condition.

602 **Differential Expression analyses**

603 Illumina RNA-seq reads were mapped to the mouse reference genome (GRCm38, ENSEMBL, release 94)
604 using the STAR aligner (v 2.7.6a)³⁶. Read counts were assigned to genes using featureCounts from Subread
605 package (v. 2.0.1) with options -Q 10 -p -B -C -s 2 -g gene_id -t exon and respective annotation file
606 (Gencode vM25). Multimappers and reads overlapping multiple features were not counted. Nanopore reads
607 counts were derived from the nanopolish-polya output files, used for the poly(A) tail lengths analyses.

608 Differential expression analysis was performed with DESeq2 (v. 1.22) Bioconductor package³⁷, using
609 LikeLikelihood Ratio test for time-course experiments data. Genes with similar expression patterns were
610 clustered with hierarchical clustering using ward.D method and Z-scored expression values for each gene.
611 Heatmaps were drawn with the ComplexHeatmap package³⁸. Gene Ontology enrichment analysis was done
612 with g:Profiler³⁹.

613 **Statistics and reproducibility.**

614 No statistical method was used to predetermine sample size. Statistical analysis was conducted on data from
615 two or more biologically independent experimental replicates. Statistical analysis of quantitative data was
616 performed using R environment unless otherwise stated. The statistical tests used in each instance are
617 mentioned in the figure legends. All data were checked for normality using the Shapiro–Wilk test. Data are
618 presented as scatter dot plots with mean values indicated and standard errors shown as the error bars, as
619 indicated in the figure legends, and individual data points are shown. Most of the experiments were repeated
620 at least twice, leading to comparable results with exception of mRNA-1273 treatment of A549 cells and
621 viability assays, which were repeated once. Samples with clear technical failures during tissue harvesting,
622 cells isolation, processing, or data collection were excluded from analyses.

623 **Data availability**

624 Nanopore direct RNA sequences are deposited at the European Nucleotide Archive; accession
625 number PRJEB53190. mRNA expression data are deposited in GEO. Raw data underlying
626 figures are provided in ED Fig. 6 and Supplementary Datasets or are also available from the
627 corresponding authors upon reasonable request.

628

629 **Code availability**

630 Dynamic Time Warping script is available at [https://github.com/LRB-IIMCB/DTW_mRNA-](https://github.com/LRB-IIMCB/DTW_mRNA-1273)
631 [1273](https://github.com/LRB-IIMCB/nanopolish_mRNA-1273). Nanopolish-polya for identification of mΨCmΨAG is available at [https://github.com/LRB-](https://github.com/LRB-IIMCB/nanopolish_mRNA-1273)
632 [IIMCB/nanopolish_mRNA-1273](https://github.com/LRB-IIMCB/nanopolish_mRNA-1273).

633

634
635
636
637
638
639
640
641
642
643
644
645
646
647
648
649
650
651
652
653
654
655
656

REFERENCES

1. Corbett, K. S. *et al.* SARS-CoV-2 mRNA Vaccine Design Enabled by Prototype Pathogen Preparedness. *Nature* **586**, 567–571 (2020).
2. Sahin, U. *et al.* BNT162b2 vaccine induces neutralizing antibodies and poly-specific T cells in humans. *Nature* **595**, 572–577 (2021).
3. Sahin, U., Karikó, K. & Türeci, Ö. mRNA-based therapeutics — developing a new class of drugs. *Nat Rev Drug Discov* **13**, 759–780 (2014).
4. Szabó, G. T., Mahiny, A. J. & Vlatkovic, I. COVID-19 mRNA vaccines: Platforms and current developments. *Molecular Therapy* **30**, 1850–1868 (2022).
5. Li, C. *et al.* Mechanisms of innate and adaptive immunity to the Pfizer-BioNTech BNT162b2 vaccine. *Nat Immunol* 1–13 (2022) doi:10.1038/s41590-022-01163-9.
6. Lindsay, K. E. *et al.* Visualization of early events in mRNA vaccine delivery in non-human primates via PET–CT and near-infrared imaging. *Nat Biomed Eng* **3**, 371–380 (2019).
7. Ols, S. *et al.* Route of Vaccine Administration Alters Antigen Trafficking but Not Innate or Adaptive Immunity. *Cell Reports* **30**, 3964-3971.e7 (2020).
8. Verbeke, R., Hogan, M. J., Loré, K. & Pardi, N. Innate immune mechanisms of mRNA vaccines. *Immunity* **55**, 1993–2005 (2022).
9. Liang, F. *et al.* Efficient Targeting and Activation of Antigen-Presenting Cells In Vivo after Modified mRNA Vaccine Administration in Rhesus Macaques. *Molecular Therapy* **25**, 2635–2647 (2017).
10. Diken, M. *et al.* Selective uptake of naked vaccine RNA by dendritic cells is driven by macropinocytosis and abrogated upon DC maturation. *Gene Ther* **18**, 702–708 (2011).

- 657 11. Kranz, L. M. *et al.* Systemic RNA delivery to dendritic cells exploits antiviral defence for
658 cancer immunotherapy. *Nature* **534**, 396–401 (2016).
- 659 12. Karikó, K. *et al.* Incorporation of Pseudouridine Into mRNA Yields Superior
660 Nonimmunogenic Vector With Increased Translational Capacity and Biological Stability.
661 *Molecular Therapy* **16**, 1833–1840 (2008).
- 662 13. Svitkin, Y. V. *et al.* N1-methyl-pseudouridine in mRNA enhances translation through eIF2 α -
663 dependent and independent mechanisms by increasing ribosome density. *Nucleic Acids*
664 *Research* **45**, 6023–6036 (2017).
- 665 14. Anderson, B. R. *et al.* Incorporation of pseudouridine into mRNA enhances translation by
666 diminishing PKR activation. *Nucleic Acids Research* **38**, 5884–5892 (2010).
- 667 15. Andries, O. *et al.* N1-methylpseudouridine-incorporated mRNA outperforms pseudouridine-
668 incorporated mRNA by providing enhanced protein expression and reduced immunogenicity
669 in mammalian cell lines and mice. *Journal of Controlled Release* **217**, 337–344 (2015).
- 670 16. Gebre, M. S. *et al.* Optimization of non-coding regions for a non-modified mRNA COVID-
671 19 vaccine. *Nature* **601**, 410–414 (2022).
- 672 17. Lutz, J. *et al.* Unmodified mRNA in LNPs constitutes a competitive technology for
673 prophylactic vaccines. *npj Vaccines* **2**, 1–9 (2017).
- 674 18. Vogel, A. B. *et al.* BNT162b vaccines protect rhesus macaques from SARS-CoV-2. *Nature*
675 **592**, 283–289 (2021).
- 676 19. Corbett, K. S. *et al.* mRNA-1273 protects against SARS-CoV-2 beta infection in nonhuman
677 primates. *Nat Immunol* **22**, 1306–1315 (2021).
- 678 20. Xia, X. Detailed Dissection and Critical Evaluation of the Pfizer/BioNTech and Moderna
679 mRNA Vaccines. *Vaccines* **9**, (2021).

- 680 21. Gagne, M. *et al.* mRNA-1273 or mRNA-Omicron boost in vaccinated macaques elicits
681 similar B cell expansion, neutralizing responses, and protection from Omicron. *Cell* **185**,
682 1556-1571.e18 (2022).
- 683 22. Garalde, D. R. *et al.* Highly parallel direct RNA sequencing on an array of nanopores.
684 *Nature Methods* **15**, 201–206 (2018).
- 685 23. Fleming, A. M. & Burrows, C. J. Nanopore sequencing for N1-methylpseudouridine in RNA
686 reveals sequence-dependent discrimination of the modified nucleotide triphosphate during
687 transcription. 2022.06.03.494690 Preprint at <https://doi.org/10.1101/2022.06.03.494690>
688 (2022).
- 689 24. Kovaka, S., Fan, Y., Ni, B., Timp, W. & Schatz, M. C. Targeted nanopore sequencing by
690 real-time mapping of raw electrical signal with UNCALLED. *Nat Biotechnol* **39**, 431–441
691 (2021).
- 692 25. Workman, R. E. *et al.* Nanopore native RNA sequencing of a human poly(A) transcriptome.
693 *Nat Methods* 1–9 (2019) doi:10.1038/s41592-019-0617-2.
- 694 26. Liudkovska, V. *et al.* TENT5 cytoplasmic noncanonical poly(A) polymerases regulate the
695 innate immune response in animals. *Science Advances* **8**, eadd9468 (2022).
- 696 27. Gewartowska, O. *et al.* Cytoplasmic polyadenylation by TENT5A is required for proper
697 bone formation. *Cell Reports* **35**, 109015 (2021).
- 698 28. Bilska, A. *et al.* Immunoglobulin expression and the humoral immune response is regulated
699 by the non-canonical poly(A) polymerase TENT5C. *Nature Communications* **11**, 2032
700 (2020).
- 701 29. Beck, J. D. *et al.* mRNA therapeutics in cancer immunotherapy. *Molecular Cancer* **20**, 69
702 (2021).

- 703 30. Rauch, S. *et al.* mRNA-based SARS-CoV-2 vaccine candidate CVnCoV induces high levels
704 of virus-neutralising antibodies and mediates protection in rodents. *npj Vaccines* **6**, 1–9
705 (2021).
- 706 31. Mroczek, S. *et al.* The non-canonical poly(A) polymerase FAM46C acts as an onco-
707 suppressor in multiple myeloma. *Nature Communications* **8**, 619 (2017).
- 708 32. Amend, S. R., Valkenburg, K. C. & Pienta, K. J. Murine Hind Limb Long Bone Dissection
709 and Bone Marrow Isolation. *JoVE (Journal of Visualized Experiments)* e53936 (2016)
710 doi:10.3791/53936.
- 711 33. Bertović, I., Bura, A. & Jurak Begonja, A. Developmental differences of in vitro cultured
712 murine bone marrow- and fetal liver-derived megakaryocytes. *Platelets* **33**, 887–899 (2022).
- 713 34. Martin, M. Cutadapt removes adapter sequences from high-throughput sequencing reads.
714 *EMBnet.journal* **17**, 10–12 (2011).
- 715 35. Wagih, O. ggseqlogo: a versatile R package for drawing sequence logos. *Bioinformatics* **33**,
716 3645–3647 (2017).
- 717 36. Sikorski, P. J. *et al.* The identity and methylation status of the first transcribed nucleotide in
718 eukaryotic mRNA 5' cap modulates protein expression in living cells. *Nucleic Acids*
719 *Research* **48**, 1607–1626 (2020).
- 720 37. Meert, W., Hendrickx, K., van Craenendonck, T. & Robberechts, P. DTAIDistance (Version
721 v2.3.5). (2022) doi:10.5281/zenodo.5901139.
- 722 38. Dobin, A. *et al.* STAR: ultrafast universal RNA-seq aligner. *Bioinformatics* **29**, 15–21
723 (2013).
- 724 39. Love, M. I., Huber, W. & Anders, S. Moderated estimation of fold change and dispersion for
725 RNA-seq data with DESeq2. *Genome Biology* **15**, 550 (2014).

- 726 40. Gu, Z., Eils, R. & Schlesner, M. Complex heatmaps reveal patterns and correlations in
727 multidimensional genomic data. *Bioinformatics* **32**, 2847–2849 (2016).
- 728 41. Raudvere, U. *et al.* g:Profiler: a web server for functional enrichment analysis and
729 conversions of gene lists (2019 update). *Nucleic Acids Research* **47**, W191–W198 (2019).
- 730
- 731

732 **Acknowledgments**

733 We thank Dziembowski lab members and IIMCB core facilities for help in selected experiments,
734 Dr Małgorzata Piotrowska from the Medical Center of the Medical University of Warsaw for
735 providing remnant vaccines and members of the Laboratory of RNA Biology, IIMCB, for help
736 with vaccination experiments. *Tent5a*^{-/-} and *Tent5a*^{Flox/Flox}/*Tent5c*^{-/-} mice were generated by the
737 Genome Engineering Unit, IIMCB. Illumina sequencing was carried out by Genomics Core
738 Facility, Centre of New Technologies, University of Warsaw (RRID:SCR_022718).

739 This work was supported by: the Virtual Research Institute, Polish Science Fund (to A.D, S.M,
740 D.N., J.G., J.K. and J.J.); Foundation for Polish Science, financed by the European Union via the
741 European Regional Development Fund (agreement no. TEAM/2016-1/3 to A/D) and National
742 Science Center (SONATA BIS 10 2020/38/E/NZ2/00372 to S.M, OPUS 17
743 2019/33/B/NZ2/01773 to A.D., SONATA 16 2020/39/D/NZ2/0217 to A.T, and PRELUDIUM 19
744 2020/37/N/NZ2/02893 to A.B.). This research was supported by funding from the European Union
745 Horizon 2020 research and innovation programme, under grant agreement no 810425.

746

747 **Author Information**

748 These authors contributed equally: Olga Gewartowska, Michal Mazur, Wiktoria Orzel

749 Contributions:

750 A.D., S.M. conceived and designed the project. P.K. developed bioinformatic tools and analyzed
751 all sequencing data. S.M. established the BMDM cultures, performed all cell line experiments, and
752 isolated RNA for DRS. O.G. performed mice immunizations, serum collection, and ELISA
753 measurements. W.O. carried out RNA isolation, DRS library preparation and sequencing, and 3'-
754 RACE-seq experiment. M.M. did RNA isolation from injection sites and qPCRs. A.T. established

755 the HEK293T CNOT1 KD cell line. K.M-K. prepared poly(A) length standards and participated
756 in I-tailing experiment (together with W.O.). T.S. prepared the fluc spike-in. P. T., D.N, and J.G.
757 provided the BMDC cultures. B.T. took part in immunization experiments. A.B. established the
758 *Tent5a^{Flox/Flox}/Tent5c^{-/-}* BMDMs cultures. S.J. did qPCRs on varying amounts of mRNA-1273 in
759 HEK293T and A549 cells. J.K., J.G, K.M.K and S.M. provided feedback on the manuscript. A.D.
760 and S.M supervised the work. P.K. and A.D wrote the manuscript, with contributions from other
761 authors. All authors read and approved the manuscript.

762 Corresponding Authors:

763 Correspondence to: Andrzej Dziembowski (adziembowski@iimcb.gov.pl) or Seweryn Mroczek
764 (s.mroczek2@uw.edu.pl)

765

766 **Ethics declarations**

767 Competing Interests

768 Jacek Jemielity, Joanna Kowalska, Jakub Gołąb, and Dominika Nowis are founders of
769 ExploRNA Therapeutics and Paweł Turowski is an employee of ExploRNA Therapeutics.

770

771 **Figure legends**

772

773 **Figure 1. Enhanced Direct RNA Sequencing (eDRS) of mRNA-1273.**

774 **a**, Overview of DRS. Library with DNA adaptor ligated to native mRNAs is loaded on the flowcell
775 with protein pores (yellow) embedded in the membrane. RNA molecules are translocated from the
776 3' end through the pore due to electric potential and activity of the motor protein (grey dot). Passing
777 through the pore causes perturbation in electric current readout, further translated (basecalled) into
778 the sequence, and subsequently used for the poly(A) length calculation.

779 **b**, Read lengths distribution of analyzed DRS data. Blue– reads mapped to mRNA-1273 after
780 standard basecalling by Guppy. Yellow– reads identified as mRNA-1273 using Dynamic Time
781 Warping (sDTW) approach. Grey – reads not attributed to mRNA-1273 (too low quality). Bin
782 width = 100, stacked histogram.

783 **c**, Distribution of poly(A) lengths for mRNA-1273 with (blue) and without (red) 3' terminal
784 m Ψ Cm Ψ AG. Bottom panel – fraction of reads in each group is indicated.

785 **d**, Representative raw signals from eDRS showing mRNA-1273 with and without 3' terminal
786 m Ψ Cm Ψ AG, bottom and top panels, respectively. Signal from poly(A) is zoomed in for
787 visualization purposes. Purple– transcript body, green – poly(A), black – adaptor, pink -
788 m Ψ Cm Ψ AG.

789 **e**, Sequence logo of mRNA-1273 poly(A) 3'end obtained from 3' RACE-seq. Last 4 adenosines
790 from poly(A) tail are shown, followed by terminal nucleotides.

791

792 **Figure 2. Stability of mRNA-1273 in model cell lines is determined by the deadenylation rate.**

793 **a**, Western blots showing efficient translation of mRNA-1273 in HEK293T and A549 cells with
794 varying amounts of mRNA-1273 LNP. Asterisk indicate unspecific band.

795 **b-c**, mRNA-1273 poly(A) length distribution in HEK293T (**b**) and A549 (**c**) cells treated with the
796 vaccine for up to 72 h. Reads are divided into ones with (blue) and without (red) m Ψ Cm Ψ AG
797 sequence. Lower panel shows the relative abundance of each group. Average distributions for 1
798 (A549) or 2 (HEK293T) replicates are shown. P.values were calculated using Wilcoxon test, p.
799 value adjustment with the Benjamini-Hochberg method.

800 **d**, Expression of mRNA-1273 in HEK293T cells up to 96 h after mRNA-1273 delivery. Western
801 Blot on spike protein. Asterisk indicate unspecific band.

802 **e**, mRNA-1273 poly(A) lengths distribution for HEK293T cells with tetracycline-induced
803 depletion of CNOT1 (CNOT1 KD) or controls (WT, cultured without tetracycline). Reads are
804 divided into ones with (blue) and without (red) m Ψ Cm Ψ AG sequence. Lower panel shows the
805 relative abundance of each group. P.values calculated using Wilcoxon test, p. value adjustment
806 with Benjamini-Hochberg method.

807

808 **Figure 3. mRNA-1273 poly(A) tail extension after m Ψ Cm Ψ AG removal *in vivo* and in**
809 **macrophages.**

810 **a**, Schematic representation of the vaccination experiment

811 **b**, Levels of mRNA-1273 at injection sites measured with qPCR 2, 8 and 24 h after injection of
812 mRNA-1273. All values are shown as fold change relative to 2 h timepoint. Red lines represent
813 mean values.

814 **c**, mRNA-1273 poly(A) lengths distribution at mRNA-1273 injection sites up to 24 h post-
815 injection. Average distributions for 2-3 replicates are shown. Reads are divided into ones with
816 (blue) and without (red) m Ψ Cm Ψ AG sequence. Lower panel shows the relative abundance of each

817 group. P.values calculated using Wilcoxon test, p. value adjustment with Benjamini-Hochberg
818 method.

819 **d**, Expression of mRNA-1273 in BMDMs up to 96 h after mRNA-1273 delivery. Western Blot on
820 spike protein, α -tubulin as control. Asterisk indicate unspecific band.

821 **e-f**, mRNA-1273 poly(A) lengths distribution in BMDMs (**e**) and DCs (**f**) treated with vaccine for
822 up to 72 h (DCs) or 96 h (BMDMs). Average distributions for 2 (DCs) or 3 (BMDMs) replicates
823 are shown. Reads are divided into ones with (blue) and without (red) m Ψ Cm Ψ AG sequence.
824 Lower panel shows the relative abundance of each group. P.values calculated using Wilcoxon test,
825 p. value adjustment with Benjamini-Hochberg method.

826
827 **Figure 4. Innate immune response and induction of TENT5A poly(A) polymerase after**
828 **vaccine administration.**

829 **a-b**, Genes with changed expression at injection sites (**a**) or in BMDMs (**b**) upon mRNA-1273
830 administration. Expression values were z-score normalized. Only genes with a significant change
831 in expression (LRT test $p < 0.05$) are shown. Clustering done using hclust, with ward.D method.
832 On the right, descriptions on major functionalities enriched in given cluster are shown. N=3656
833 (**a**) or 584 (**b**).

834 **c**, Transcripts with changed poly(A) lengths (revealed with Kruskal Wallis test) in the time course
835 (up to 72 h) upon mRNA-1273 administration. Z-score normalized poly(A) lengths are represented
836 in a colour-scale. Clustering done using hclust, with ward.D method. On the right, descriptions on
837 major functionalities enriched in given cluster are shown. N=124.

838 **d-e**, Expression of non-canonical poly(A)/poly(U) polymerases (**d**) or deadenylase complexes
839 subunits (**e**) in BMDMs treated with mRNA-1273 for up to 72 h. Gene names are indicated on the
840 left, on the right adjusted p.values from the DESeq2 LRT test are shown. Height of the bar indicates
841 the expression change significance. Expression is shown as DESeq2-normalized counts.

842
843 **Figure 5. TENT5 poly(A) polymerases re-adenylate mRNA-1273, enhancing antigen**
844 **production and immune response.**

845 **a**, mRNA-1273 poly(A) length distribution in BMDMs (*Tent5a^{lox/lox}/Tent5c^{-/-}*) treated with
846 vaccine for up to 72 h. Average distributions for 2 replicates are shown. Reads are divided into
847 ones with (blue) and without (red) m Ψ Cm Ψ AG sequence. Lower panel shows the relative
848 abundance of each group. P.values calculated using Wilcoxon test, p. value adjustment with
849 Benjamini-Hochberg method.

850 **b**, Stability of mRNA-1273 in WT (black) or *Tent5a^{lox/lox}/Tent5c^{-/-}* (red) BMDMs (based on eDRS,
851 refer to Fig. 3e and Fig. 5a). Abundance of mRNA-1273 normalized to 24 h timepoint. Standard
852 errors are shown as error bars.

853 **c**, Model of action of TENT5 poly(A) polymerases, which target transcripts encoding proteins
854 translated on the endoplasmic reticulum (ER).

855 **d**, Overview of the immunization experiment.

856 **e**, Spike protein levels in serum of immunized mice, WT and *Tent5a^{-/-}*, measured 4 days after
857 immunization. Red lines represent mean values.

858 **f**, Anti-spike IgG levels in serum of immunized mice, WT and *Tent5a^{-/-}*, measured 14 days after
859 immunization. Values are shown in relation to overall IgG levels (refer to ED Fig. 5g). Red lines
860 represent mean values.

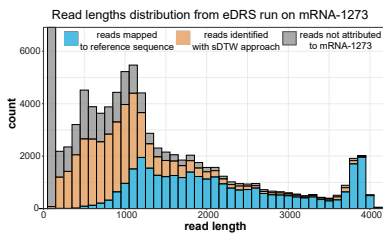
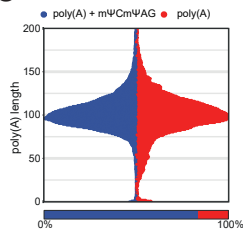
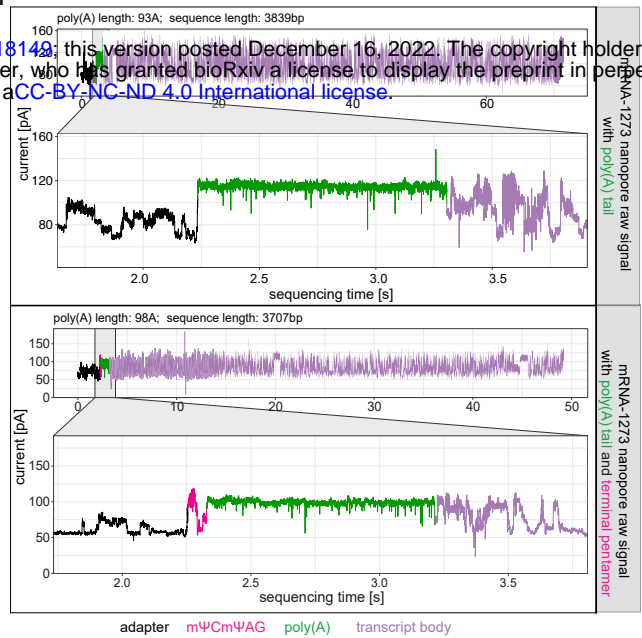
861 **g**, Correlation scatterplot showing relation between spike protein level at day 4 post-immunization
862 and anti-spike IgG levels at day 14 post-immunization.

863

a

AGUCCAGUGCAGCAGUGCAU
 sequence (basecalling)

poly(A) length

b**c****d****e**